IEEE Access
Multidisciplinary ⋮ Rapid Review ⋮ Open Access Journal

Received 2 July 2023, accepted 27 July 2023, date of publication 7 August 2023, date of current version 16 August 2023.

Digital Object Identifier 10.1109/ACCESS.2023.3303259

RESEARCH ARTICLE

Reconfigurable Multiband Antenna Booster Architecture for Different Environments

ALEJANDRO FERNÁNDEZ[1], AURORA ANDÚJAR[1], JOAN LLUÍS PIJOAN[2], AND JAUME ANGUERA[1,2], (Fellow, IEEE)

[1]Ignion, 08174 Barcelona, Spain
[2]Research Group on Smart Society, La Salle Engineering, Universitat Ramon Llull, 08022 Barcelona, Spain

Corresponding author: Jaume Anguera (jaume.anguera@ignion.io)

This work was supported in part by the Industrial Doctorate Plan of the Secretariat of Universities and Research of the Department of Business and Knowledge of the Generalitat of Catalonia under Grant Reference 2021 DI 115.

ABSTRACT A passive matching network cannot match a device for more than one specific scenario. For this reason, a new approach capable of matching a 50 mm × 50 mm Internet of Things (IoT) device at 698-960 MHz and 1710-2170 MHz, using a single SP4T (Single Pole 4 Throw) switch to provide good impedance matching ($|S_{11}| < -6$ dB), across five different environment cases (free space, metal, bricks, wood, and human body), is presented. To validate the capabilities of the proposed reconfigurable matching network to match the surrounding environments, two extreme scenarios have been considered: 1) at free space and 2) when the prototype is placed at three different h distances of 7, 15, and 20 mm (0.016 λ, 0.035 λ, and 0.046 λ, respectively, at the lower frequency of operation of 698 MHz) from four different materials: metal, bricks, wood, and human body. The proposed method can compensate for the effects of the close environment variations by commuting between matched states of the reconfigurable matching network. To validate it, a prototype is implemented and tested in all the enumerated materials. By using the proposed reconfigurable architecture, total efficiency is maximized in all cases. The total efficiency increased by 0.8 dB for the on-wood case, by 1.7 dB for the on-body case, by 1.9 dB for the on-brick case, and by 3 dB for the on-metal case compared to a solution where the same matching network is used for all cases.

INDEX TERMS Small and multiband antennas, reconfigurable architecture, antenna booster, the IoT.

I. INTRODUCTION

IoT devices are intended to be used in different environments, in many of which the device may be in a critical position in terms of radio frequency. For example, placing the device on the metallic surface of a shipping container, a car, or a washing machine results in severe signal attenuation and frequency shifting [1], [2], [3]. To solve it, a new approach capable of counterbalancing the frequency shift produced by the variation of the close environment surrounding the IoT device is proposed.

Reconfigurable solutions are attractive to provide multiband operation [4], [5], [6], [7], [8], [9], [10], [11], [12], [13], [14]. In [4], a Digitally Tunable Capacitor (DTC) to reconfigure the operating frequency of the device is proposed, and in [10], a DTC is used to counterbalance the shift of the antenna resonant frequency produced by the variation of the close surrounding of the IoT device. In [11], diodes are included to modify the geometry of a low-profile branched monopole antenna to achieve multiband operation in six different bands. In this paper, however, the proposed architecture employs a reconfigurable architecture providing not only multiband operation across the frequency range of 698-960 MHz and 1710-2170 MHz where IoT protocols, such as NB-IoT or LTE-M are allocated but also providing a good impedance match ($|S_{11}| < -6$ dB) when the device is exposed to the effect of different materials in very close proximity, such as wood, brick, metal, and the human body. By commuting between states, the best impedance matching for each environment is achieved. To have as realistic device locations as possible, three different spacings ($h = 7$ mm, $h = 15$ mm, and $h = 20$ mm) have been used for each

The associate editor coordinating the review of this manuscript and approving it for publication was Giovanni Pau.

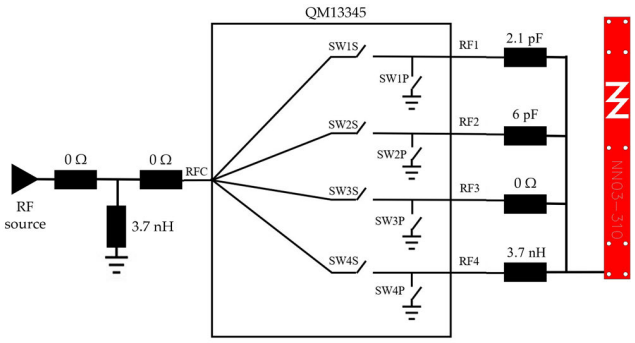

FIGURE 1. Proposed reconfigurable architecture. Note that the Π-type matching network between the RF source and the SP4T only needs a shunt inductor; the 0Ω allows an extra degree of freedom for further impedance tuning if needed in the prototyping phase.

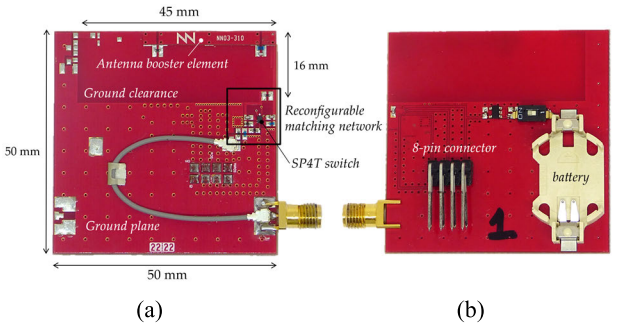

FIGURE 2. A 30 mm × 3 mm × 1 mm antenna booster element on a 50 mm × 50 mm PCB comprising a 45 mm × 16 mm ground clearance and a reconfigurable architecture: with an SP4T switch and lumped SMD components for multiband performance at 698-960 MHz and 1710-2170 MHz. (a) top view. (b) rear view.

material. A reconfigurable architecture capable of matching 12 different environments (4 materials × 3 h distances) and free space is presented.

The proposed reconfigurable multiband architecture is (Fig. 1) obtained by adding a reconfigurable element (an SP4T switch) to an antenna booster element. The antenna booster element [15] is a non-resonant element at the low frequencies of operation, where the addition of a matching network easily adjusts the frequencies of operation [16].

This paper is structured as follows: the need for a reconfigurable matching network design in different materials is analyzed in section II. The proposed reconfigurable architecture is presented in section III. The results are shown in section IV. A discussion of some representative cases is provided in section V. Finally, conclusions are drawn in section VI.

II. THE NEED FOR RECONFIGURABILITY

The basic approach to matching an antenna booster element to the desired frequency region is to use a passive matching network [17], [18]. In this section, the need for reconfigurability is analyzed. In the first case, a matching network is designed to match the device for a free-space scenario. In a second case, a matching network is designed considering the device on top of a conductive body.

The prototype created for this analysis has a dimension of 50 mm × 50 mm and a ground clearance of 45 mm × 16 mm (Fig. 2). The 30 mm × 3 mm × 1 mm (height) antenna booster element is placed at the corner. For simulation purposes, the antenna booster element is available for CST Microwave Studio [19].

A 2-component passive matching network (Fig. 3. a), able to match the prototype at free space for the frequency region of 698-750 MHz, is proposed.

The S-parameter of the printed circuit board (PCB) shown in Fig. 2 is measured with a Vector Network Analyzer (VNA) in free space and $h = 7$ mm on top of a 400 mm × 400 mm metallic plate (Fig. 4) at 698-750 MHz, without any matching network. The distance h is the spacing between the PCB and the metallic plate. This spacing is representative of a real case because batteries, as well as other components, will be integrated below the ground plane of the device. For each situation, a matching network is designed to match the non-resonant capacitive impedance of the antenna booster element. When using the same free-space matching network in the on-metal case, the impedance is no longer matched but shifted to a lower impedance. This is consistent with antenna theory, when a horizontal current element is electrically close to a perfect electric conductor, the radiation efficiency and impedance decrease [20]. Thus, S_{11} degrades to –2 dB (Fig. 3. b). If the exercise is repeated but with a matching network for the on-metal case (Fig. 3. c), the matching is acceptable ($|S_{11}| < -6$ dB). However, the free space case is no longer matched (Fig. 3. d). Therefore, a passive matching network cannot meet a good match for both situations.

The same conclusion is achieved when the h distance from the metallic layer is increased to 15 and 20 mm. Even though the shift is reduced as the distance from the metallic plate increases, a new matching network for each distance is needed to achieve the best match. Indeed, when the material is changed, the same problem appears.

To overcome this drawback, a reconfigurable architecture is designed, where the tunable architecture provides enough degrees of freedom to match both free-space and on-metal cases. Furthermore, the architecture is also able to provide multiband operation across 698-960 MHz and 1710-2170 MHz for both free-space and on-metal cases and even for three new scenarios (on-wood, on-brick, and on-body), as explained in the next section.

III. PROPOSED RECONFIGURABLE ARCHITECTURE

The proposed reconfigurable architecture is designed to combine an antenna booster element with the addition of a tunable element, an SP4T switch (Fig. 1). It consists of strategically arranging the outputs of the SP4T switch with series lumped components to an off-the-shelf antenna booster element. Thanks to the shunt switches of the SP4T switch, not only series matching networks are possible, but also a shunt-series

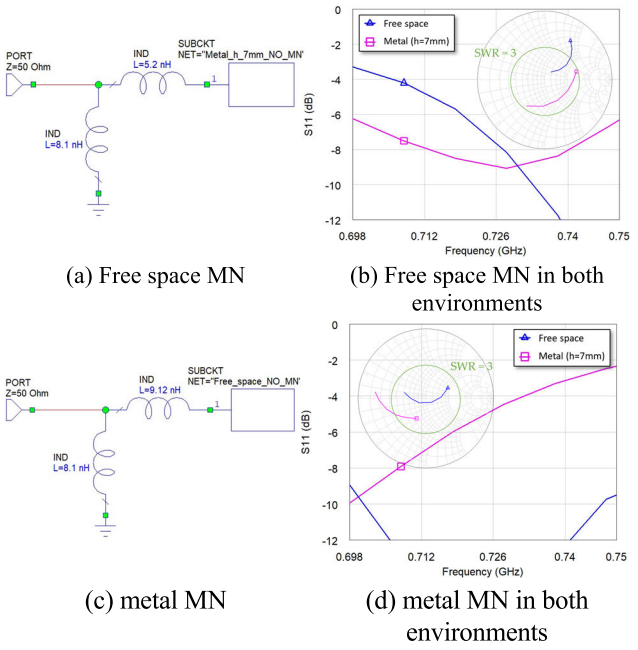

FIGURE 3. Simulated S_{11} of a 2-component matching network (MN) from the S-parameters of the proposed prototype (Fig. 2) at free space and 7 mm on top of a metallic layer (Fig. 4) from 698-750 MHz. (a) free space MN. (b) both environments with a matching network designed for free space. (c) metallic environment MN. (d) both environments with a matching network designed for the metallic environment. Simulations are done with AWR Microwave Office.

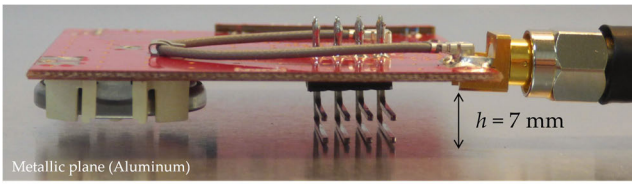

FIGURE 4. Side view of the proposed prototype (Fig. 2) 7 mm on top of a 400 mm × 400 mm metallic layer.

(the shunt is the one connected to the antenna booster elements). The SP4T switch has eight internal switches, achieving 28 = 256 different switch states. Of those 256 states, some of them are not useful. For example, when SW1S, SW2S, SW3S, and SW4S are opened, no matter the state of the SWiP (i = 1, 2, 3, 4), the result is an open circuit. When any of the series and the corresponding shunt switch are on, it is also not useful since this is in a short circuit state. After applying all combinations, it results in 65 useful states (15 series combinations and 50 having a shunt-series topology).

This element allows 65 passive matching networks to be grouped in a single reconfigurable architecture, providing the ability to use different states of the switch for each environment [21]. For this prototype, 12 cases (on-wood, on-brick, on-metal, and on-body for a distance *h* of 7, 15, and 20 mm from the material) plus free space are used. Still, this experiment could be extrapolated to other environments. In the end, only 25 states are needed.

A multiband reconfigurable architecture (Fig. 1) able to cover 698-960 MHz and 1710-2170 MHz, providing good

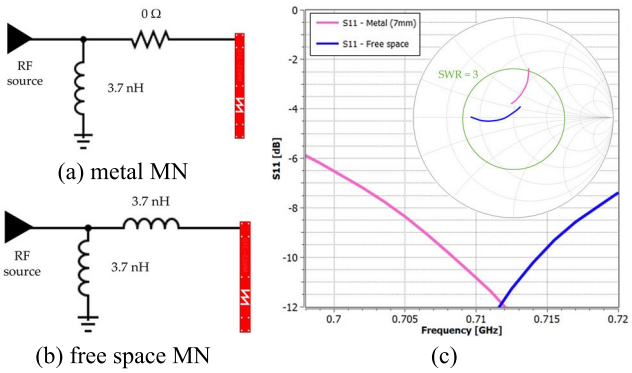

FIGURE 5. (a) Matching network for 698-720 MHz from the proposed reconfigurable architecture (Fig. 1) used when the prototype is over a metallic layer (Fig. 4). (b) for free space. (c) Measured S_{11} for the proposed prototype (Fig. 2) from 698-720 MHz.

impedance matching ($|S_{11}| < -6$ dB) no matter the environment, is presented. All selected part numbers of the lumped SMD components have a Q value greater than 60 at the frequency of operation. The prototype matching network has a Π-type matching network designed to have more flexibility when matching the prototype, but only one shunt inductor was needed, which is the reason for 0 Ohms series resistors.

The SP4T switch allows several states to be matched for free space and other scenarios, i.e., when the prototype is placed 7 mm from a metallic plate, achieving a good impedance matching ($|S_{11}| < -6$ dB) with the same reconfigurable matching network. Following the same example used in section II, for the frequency region of 698-720 MHz, the proposed reconfigurable matching network uses state #4 (Fig. 5. a) when the prototype is 7 mm on top of a metallic layer and state #8 (Fig. 5. b) when the prototype is in free space. In both cases, the prototype can be matched below –6 dB of S_{11} (Fig. 5. c).

The selected SP4T switch is the QM13345 from Qorvo, which has a dimension of 1.1 mm × 1.5 mm × 0.4 mm (height), and it is software-controlled through a parallel MIPI interface by connecting the prototype to Qorvo's software through the 8-pin connector located at the rear ground plane of the PCB (Fig. 2. b). Since the ground plane is a relevant element for the radiation process, to carry a measurement, the prototype should not have any interface bus connected that may degrade the total efficiency measurements. Therefore, to remove any cable from the prototype that may interfere with the efficiency testing, a tiny battery is embedded at the rear ground plane of the PCB. Since the switch receives the DC voltage from the battery, the state is maintained, and both S_{11} and total efficiency measurements can be carried out without the impact of the interface bus connection. The use of the small battery, even though it has an impact on the currents of the PCB, it provides the advantage of avoiding the use of the interface to power the switch, which would lead to an inaccurate measurement given the small antenna dimensions compared to the operating wavelength.

With the proposed approach, the prototype achieves an acceptable match ($|S_{11}| < -6$ dB) not only in both free space and on-metal environments but also on-wood, on-brick, and on-body. Indeed, the average measured total efficiency is doubled at 698-960 MHz when comparing free-space switch states versus on-metal switch states at 7 mm on top of a metallic plate (further discussion will be made in section V).

For the free-space scenario, the components of the matching network are obtained through matching network synthesis with Optenni-Lab. For the other scenarios, other states have been explored to finally pick those with better impedance matching.

IV. RESULTS

This section shows the results obtained when measuring the prototype (Fig. 2) with the proposed multiband reconfigurable architecture (Fig. 1), covering 698-960 MHz and 1710-2170 MHz, at free space and h mm on top of all four different materials: wood, metal, brick, and human body.

The reconfigurable architecture is capable of properly matching ($|S_{11}| < -6$ dB) when located in free space and at 7, 15, and 20 mm on top of a metallic layer, a wooden plate, bricks, and a body phantom. By commuting between matched switch states for each of the cases, the best adaptation for each environment is achieved.

To visualize the S_{11} and total efficiency results, an envelope of all the used switch states for each environment has been made. The S_{11} has been measured with a VNA, and the total efficiency (η_t) has been measured inside an anechoic chamber (Fig. 6. top) using 3D pattern integration (MVG Star-Lab 18). The total efficiency considered both the radiation efficiency (η_r) and the mismatch losses as follows: $\eta_t = \eta_r \cdot (1 - |S_{11}|^2)$. In both measurements to emulate the effect of the desired material, a plate is used (Fig. 6. bottom). To emulate the effect of a brick wall, a 400 mm × 400 mm × 38 mm (thick) brick plate with $\varepsilon_r = 3.95$ and $tan(\delta) = 0.0185$ is used (Fig. 6. a). To emulate the effect of wood, a 400 mm × 400 mm × 15 mm (thick) wooden plate with $\varepsilon_r = 1.64$ and $tan(\delta) = 0.0680$ is used (Fig. 6. b). To emulate the effect of a metallic layer, a 400 mm × 400 mm × 2 mm (thick) aluminum plate with $\sigma = 3.816 \times 10^7$ S/m is used (Fig. 6. c). To emulate the effect of the human body, a 192 mm × 105 mm × 52 mm (thick) body phantom container with $\varepsilon_r = 41.5$ and $tan(\delta) = 0.0157$ at 698-960 MHz and with $\varepsilon_r = 40.0$ and $tan(\delta) = 0.0244$ at 1710-2170 MHz is used (Fig. 6. d).

To carry the measurements with the prototype (Fig. 2), the state of Qorvo's QM13345 switch is selected using the MIPI master interface controlled by a laptop using Qorvo's application. Once the state is set, the MIPI digital cable bus can be disconnected to not interfere with the impedance and radiation measurements. The onboard battery and voltage regulator provides the required power to the switch.

A. FREE SPACE

When the prototype is located at free space, it achieves an average measured S_{11} of −10.7 dB at 698-960 MHz and

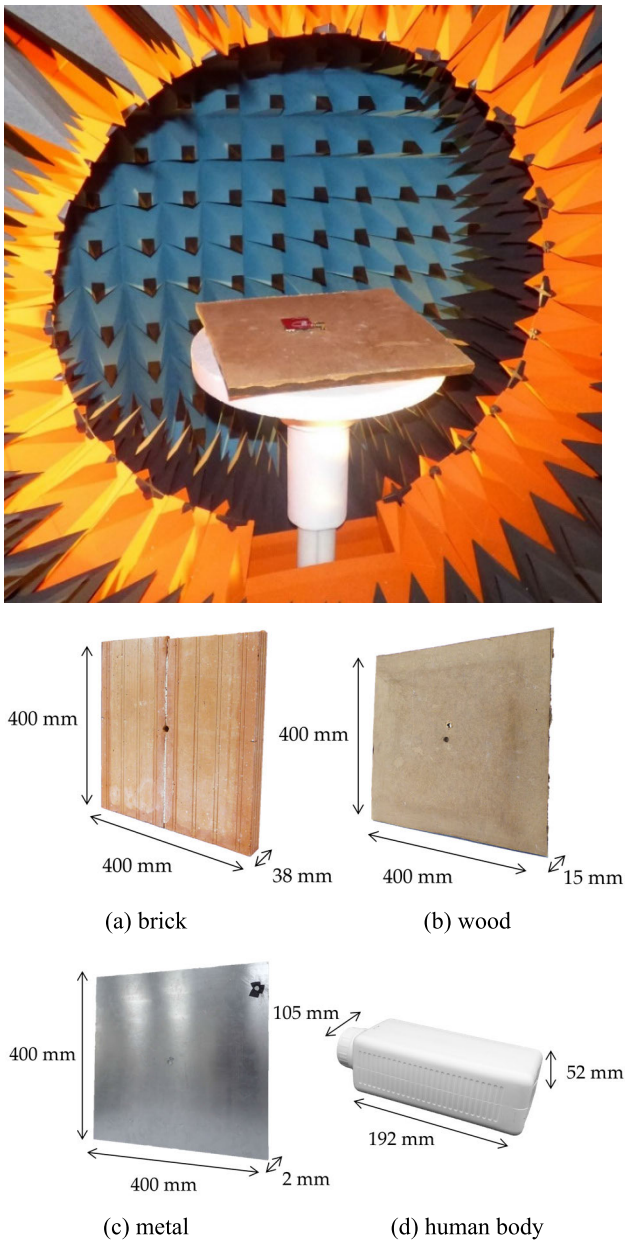

FIGURE 6. MVG Star-Lab 18 anechoic chamber setup (top) and plates used to emulate the material effect inside the anechoic chamber (bottom).

−10.4 dB at 1710-2170MHz (Fig. 7. a), with an average measured total efficiency of 26.1% and 51.2% (Fig. 7. b), respectively, showing a competitive total efficiency for such a small form factor (50 mm × 50 mm).

To achieve the best performance, the following seven states have been used to cover the low-frequency region (LFR) of 698-960 MHz: state #8 from 698-729 MHz, state #4 from 730-789 MHz, state #14 from 790-839 MHz, state #11 from 840-869 MHz, state #131 from 870-889 MHz, state #65 from 890-939 MHz and, state #129 from 940-969 MHz. To cover the high-frequency region (HFR) of 1710-2170 MHz, four states have been used: state #134 from 1710-1759 MHz, state #65 from 1760-1849 MHz, state #14

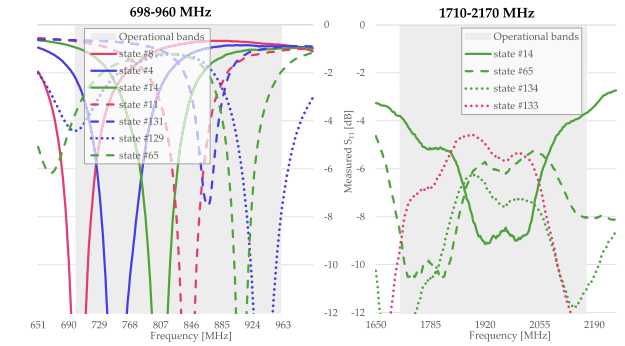

(a) S_{11}

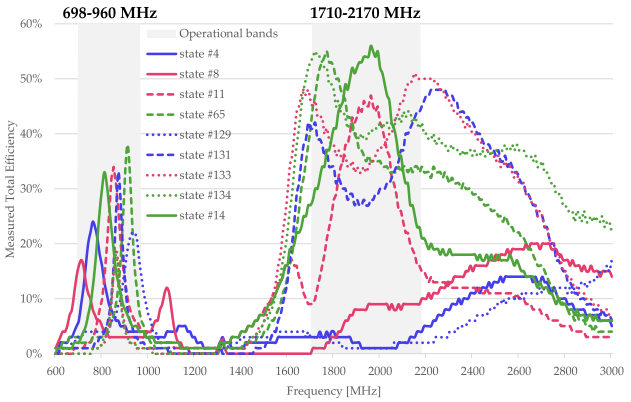

(b) Total efficiency

FIGURE 7. Measured S_{11} and total efficiency when the prototype is in free space.

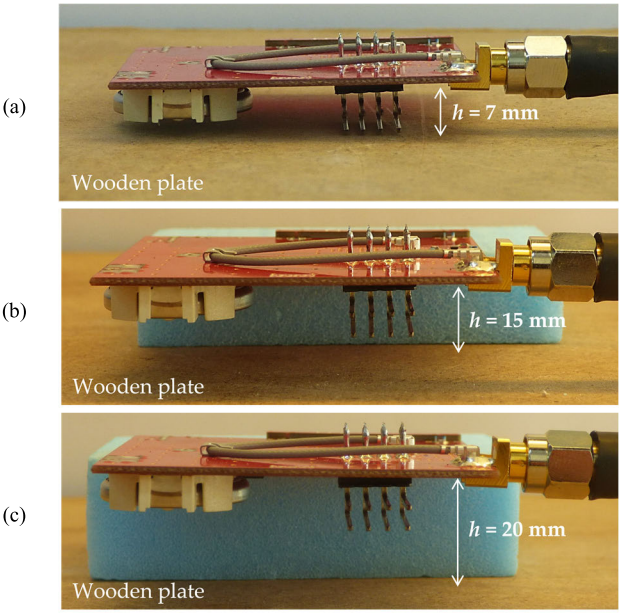

FIGURE 8. Prototype placed *h* mm on top of a 400 mm × 400 mm wooden plate. (a) *h*= 7 mm. (b) *h*= 15 mm. (c) *h* = 20 mm.

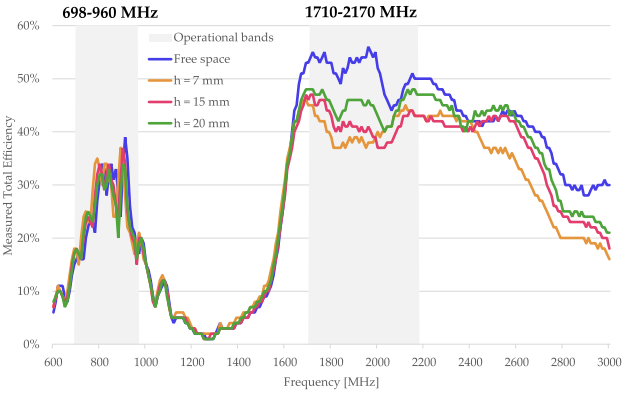

FIGURE 9. Envelope of the measured total efficiency when the prototype is placed *h* mm on top of a wooden plate (Fig. 8).

from 1850-2049 MHz and, state #133 from 2050-2170 MHz. A total of 9 different states have been used to achieve multi-band operation.

The average total efficiency of the prototype (η_t) for the LFR is $\eta_t \cong -3dB$ from which, the loses introduced from the matching network ($\eta_t = \eta_r \cdot \eta_{MN}$) (SP4T switch + lumped components) are $\eta_{MN} \cong -0.8\ dB$ and Radiation efficiency (η_r) is −2.2dB. The −2.2dB radiation efficiency is due to the small ground plane (∼50 mm x 34mm).

B. WOOD

To measure the effect of wood on the prototype, this has been placed at 7, 15, and 20 mm (Fig. 8) on top of a 400 mm × 400 mm × 15 mm (thick) wooden plate (Fig. 6. b).

For each *h* distance, to achieve the best performance, the reconfigurable architecture (Fig. 1) has been optimized by using the best-matched switch states for each frequency without changing the topology for any *h* distance.

Total efficiency results plotted in Fig. 9 show that wood does not interfere with the performance of the prototype at the LFR of 698-960 MHz. Achieving an average measured total efficiency between 25.3% and 26.5% (TABLE 1), which is very similar to the 26.1% achieved at free space. On the other hand, for the HFR of 1710-2170 MHz, wood at 7 mm from the prototype reduces the average S_{11} 0.7 dB from free space. The average total efficiency of the prototype increases with *h* (TABLE 1). When placed at 20 mm on top of the wooden plate, the reconfigurable architecture achieves an average measured S_{11} for the HFR equal to free space, −10.4 dB. But the average measured total efficiency is 6.1 points lower, meaning that even though the reconfigurable architecture can match the prototype in the presence of the material. Wood absorbs 1 dB of the average total efficiency radiated to the space at the frequency region of 1710-2170 MHz.

To sum up, wood has no impact on the performance for 698-960 MHz and absorbs, when equally matched with free space, 1 dB of the power radiated to the space at 1710-2170 MHz.

C. BRICK

To measure the effect of brick on the prototype, this has been placed at 7, 15, and 20 mm (Fig. 10) on top of a 400 mm × 400 mm × 38 mm (thick) brick plate (Fig. 6. a).

TABLE 1. Average measured S_{11} and total efficiency when the prototype is placed *h* mm on top of a wooden plate.

Average measured		698-960 MHz S_{11} [dB]	698-960 MHz Total Effi. [%]	1710-2170 MHz S_{11} [dB]	1710-2170 MHz Total Effi. [%]
Free space		–10.7	26.1	–10.4	51.2
Wood	*h* = 7 mm	–9.6	26.5	–9.7	40.5
	h = 15 mm	–10.4	25.8	–10.1	41.5
	h = 20 mm	–11.3	25.3	–10.4	45.1

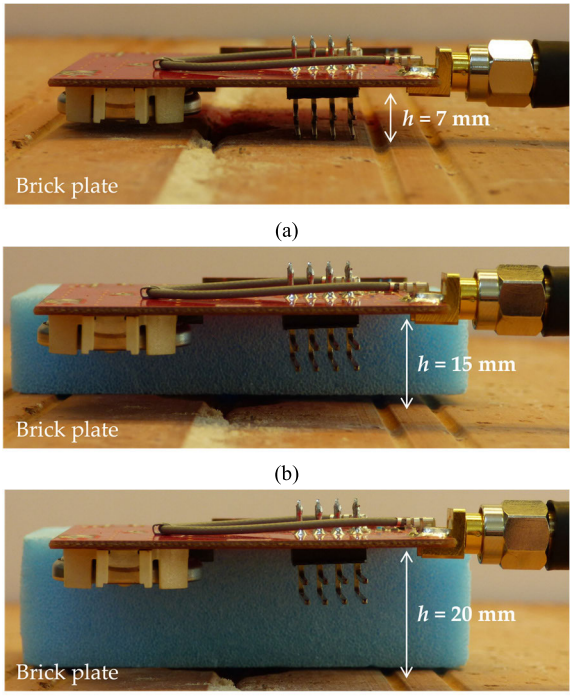

FIGURE 10. Prototype placed *h* mm on top of a 400 mm × 400 mm brick plate. (a) *h*= 7 mm. (b) *h*= 15 mm. (c) *h* = 20 mm.

For each *h* distance, to achieve the best performance, the reconfigurable architecture (Fig. 1) has been optimized by using the best-matched switch states for each frequency without changing the topology for any *h* distance.

Total efficiency results plotted in Fig. 11 show that the presence of brick near the prototype reduces the total efficiency at both bands. The reconfigurable architecture has been capable of matching the prototype with an average S_{11} comparable with the free space one for all three *h* distances (TABLE 2). Despite this, when the prototype is placed at 7 mm on top of the brick plate, the average total efficiency at the LFR is 18.9%, at 15 mm is 20.6%, and at 20 mm is 22.6% (TABLE 2). In comparison, free space is 26.1%. As the distance *h* increases, the average total efficiency improves linearly. The same happens for the HFR.

To sum up, the reconfigurable architecture can match the prototype despite the presence of brick. This presence produces attenuation of the total efficiency as the prototype is closer to the material.

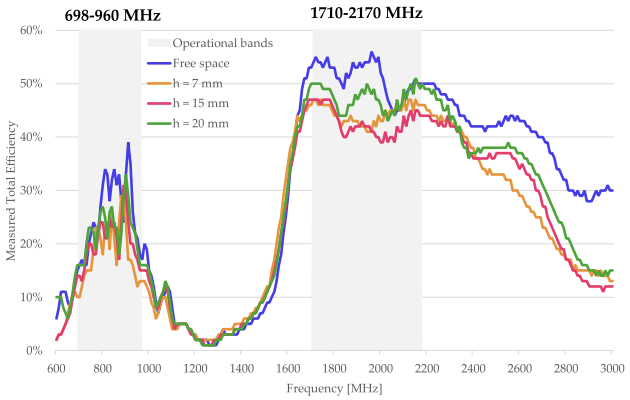

FIGURE 11. Envelope of the measured total efficiency when the prototype is placed *h* mm on top of a brick plate (Fig. 10).

TABLE 2. Average measured S_{11} and total efficiency when the prototype is placed *h* mm on top of a brick plate.

Average measured		698-960 MHz S_{11} [dB]	698-960 MHz Total Effi. [%]	1710-2170 MHz S_{11} [dB]	1710-2170 MHz Total Effi. [%]
Free space		–10.7	26.1	–10.4	51.2
Brick	*h* = 7 mm	–10.8	18.9	–10.4	44.4
	h = 15 mm	–11.4	20.6	–11.0	42.7
	h = 20 mm	–10.4	22.6	–10.6	47.3

D. METAL

To measure the effect of metal on the prototype, this has been placed at 7, 15, and 20 mm (Fig. 12) on top of a 400 mm × 400 mm × 2 mm (thick) metallic plate (Fig. 6. c).

For each *h* distance, to achieve the best performance, the reconfigurable architecture (Fig. 1) has been optimized by using the best-matched switch states for each frequency without changing the topology for any *h* distance.

Note that 7 mm is the minimum distance from the PCB to the material under study. The reason is that 7 mm is representative of the height of a battery used to power an IoT device.

Total efficiency results plotted in Fig. 13 show the attenuation and frequency shifting produced by the metallic layer. Despite that, the average S_{11} increases with the increase in the distance *h* of the prototype from the metallic layer. The prototype is not capable of matching properly in comparison with the free space case. At $h = 7$ mm, the average S_{11} at 698-960 MHz is 2 dB lower than at free space, and at 1710-2170MHz is 0.5 dB lower (TABLE 3). On the other hand, when the prototype is 20 mm on top of the metallic layer, 698-870 MHz outperformed the free space case in terms of total efficiency, achieving an average of 28.1% for the LFR, which is two points higher than the 26.1% achieved in free space. In other words, the reconfigurable architecture can overcome the frequency shifting produced by the presence of metal and achieve a proper total efficiency (in comparison with free space), despite the conductivity of the metallic layer.

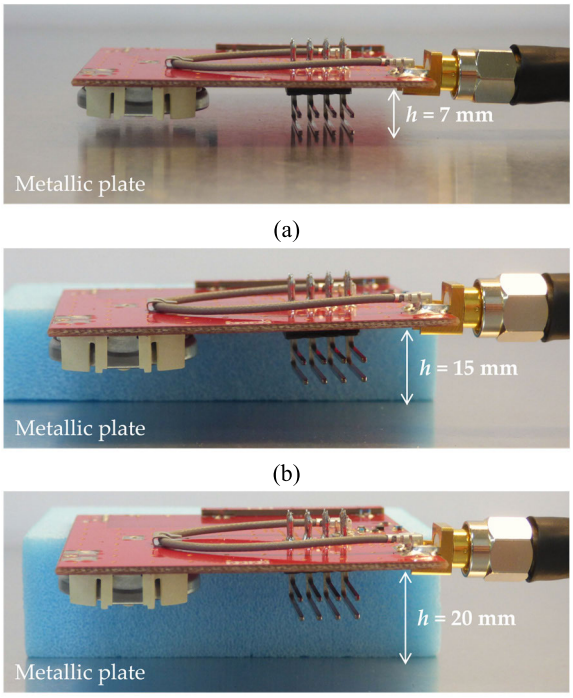

FIGURE 12. Prototype placed h mm on top of a 400 mm × 400 mm metallic plate. (a) h = 7 mm. (b) h= 15 mm. (c) h = 20 mm.

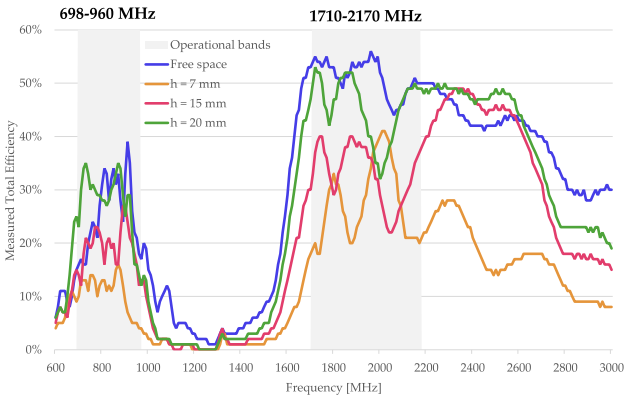

FIGURE 13. Envelope of the measured total efficiency when the prototype is placed h mm on top of a metallic plate (Fig. 12).

TABLE 3. Average measured S_{11} and Total efficiency when the prototype is placed h mm on top of a metallic plate.

Average measured		698-960 MHz		1710-2170 MHz	
		S_{11} [dB]	Total Effi. [%]	S_{11} [dB]	Total Effi. [%]
Free space		–10.7	26.1	–10.4	51.2
Metal	h = 7 mm	–8.7	10.9	–9.9	27.7
	h = 15 mm	–9.5	19.5	–10.1	33.0
	h = 20 mm	–7.6	28.1	–9.7	45.4

To sum up, the presence of metal has a significant impact even at 20 mm from the prototype. The reconfigurable architecture can reduce frequency shifting using specifically matched states for every h distance.

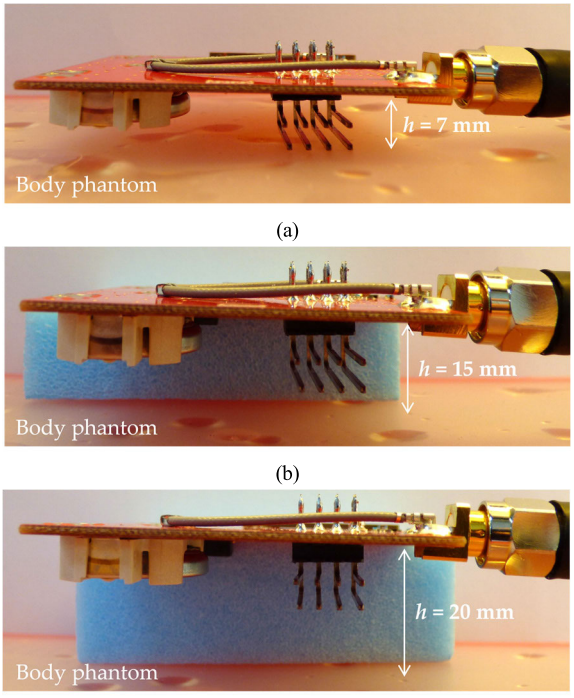

FIGURE 14. Prototype placed h mm on top of a 192 mm × 105 mm × 52 mm (height) body phantom container. (a) h = 7 mm. (b) h = 15 mm. (c) h = 20 mm.

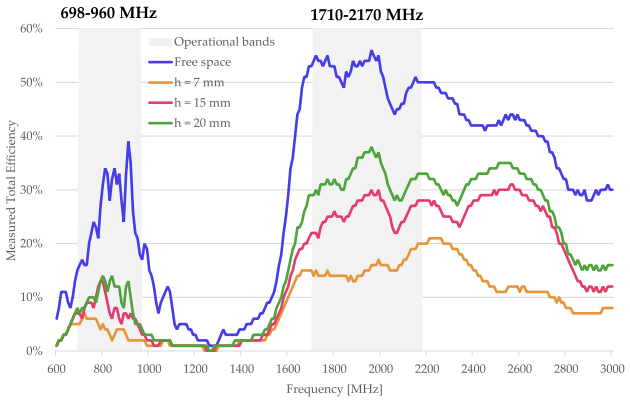

FIGURE 15. Envelope of the measured total efficiency when the prototype is placed h mm on top of a body phantom container (Fig. 14).

E. HUMAN BODY

To measure the effect of the human body on the prototype, this has been placed at 7, 15, and 20 mm (Fig. 14) on top of a 192 mm × 105 mm × 52 mm (thick) body phantom container (Fig. 6. d).

For each h distance, to achieve the best performance, the reconfigurable architecture (Fig. 1) has been optimized by using the best-matched switch states for each frequency without changing the topology for any h distance.

TABLE 4. Average measured S_{11} and total efficiency when the prototype is placed *h* mm on top of a body phantom container.

Average measured		698-960 MHz		1710-2170 MHz	
		S_{11} [dB]	Total Effi. [%]	S_{11} [dB]	Total Effi. [%]
Free space		–10.7	26.1	–10.4	51.2
Human body	h = 7 mm	–7.8	4.0	–10.0	15.4
	h = 15 mm	–8.7	7.9	–11.0	25.9
	h = 20 mm	–10.5	10.0	–10.7	32.3

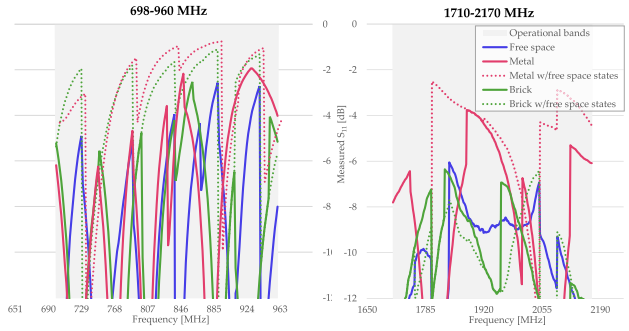

FIGURE 16. Envelope of the measured S_{11}. Comparison between optimized switch states (solid line) and free space states (dotted line). Prototype placed 7 mm on top of metal and brick.

Total efficiency results plotted in Fig. 15 show the worst total efficiency results achieved by any material in this paper. Indeed, due to the high absorption of the human body, it has the worst performance at all three h distances on all the materials studied in this article. As the distance h to the material increases, the impact of the material is reduced, improving the total efficiency. In this case, at the LFR, the average measured total efficiency increased by 2.9 dB from h= 7 mm to h= 15 mm, and by 1 dB from h= 15 mm to h= 20 mm (TABLE 4). The same happens for the HFR with 2.2 dB and 0.9 dB increases, respectively. The performance increase is smaller as the distance h increases, following a logarithmical curve. Indeed, at h = 20 mm for the LFR, the average S_{11} is comparable with the free space case, but the average total efficiency is 1.7 dB lower than the free space, proving the high absorption of the material.

To sum up, the presence of the human body has a severe impact on the performance of the prototype. Despite being well matched, the material absorbs power radiated to space.

V. DISCUSSION

This section discusses the advantages of the proposed reconfigurable architecture and compares the impact of the different environments on the performance of the prototype, showing how the reconfigurable architecture manages to improve its performance in all cases.

To prove the reconfigurability of the proposed architecture, a comparison between the static approach, which

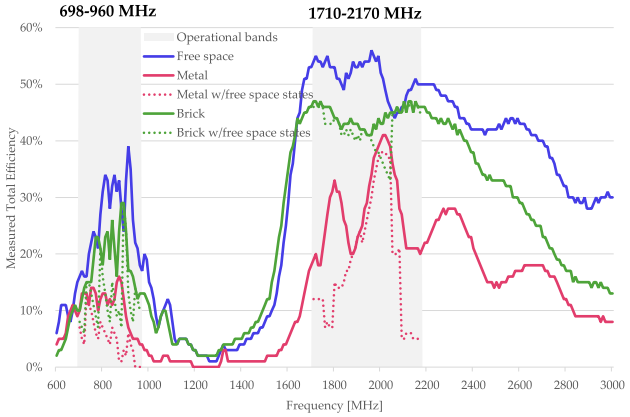

FIGURE 17. Envelope of the measured total efficiency. Comparison between optimized switch states (solid line) and free space states (dotted line). Prototype placed 7 mm on top of metal and brick.

consists of using the same matching network regardless of the environment, and the proposed reconfigurable approach has been made. A comparison between matched switch states for each material (presented in section IV) vs. the use of the same matched states for all environments to represent the static approach has been made. As discussed in section II, the static approach consists of using the same matched architecture, in this case, the free space matched states, for all cases.

When the prototype is 7 mm on top of the metallic layer (Fig. 16 – red curve), the average S_{11} at 698-960 MHz is 5.4 dB higher when using matched states than with free space states, at 1710-2170 MHz is 2.2 dB higher. The same happens when the device is 7 mm on top of a brick plate, with an average S_{11} of –4.5 dB when using the static approach (Fig. 16 – dotted green curve) and an average S_{11} of –10.8 dB with the proposed reconfigurable architecture (Fig. 16 – solid green curve) at 698-960 MHz. The average S_{11} at 1710-2170 MHz is –10.4 dB and –10.6 dB, respectively.

Those results show the improvement achieved by the reconfigurable architecture without changing the topology. Indeed, in the lower frequency region, the average S_{11} increased by 5.4 dB for metal and by 6.3 dB for brick.

For the same cases, a total efficiency comparison has been made (Fig. 17). In which it is appreciated a 3.3 dB increase in the average total efficiency for the metal case at 698-960 MHz (TABLE 5) and 1.9 dB for brick. It can be appreciated that the improvement in adaptation is not proportional to the increase in efficiency. Even though the reconfigurable architecture can mitigate the frequency shifting produced by the material using specifically matched states for every environment. The attenuation of the radiated efficiency produced by every material can only be compensated by increasing the distance h to the material, in other words, by reducing the impact of the material on the prototype.

From TABLE 5, it can be appreciated that the reconfigurable architecture has a better performance in comparison

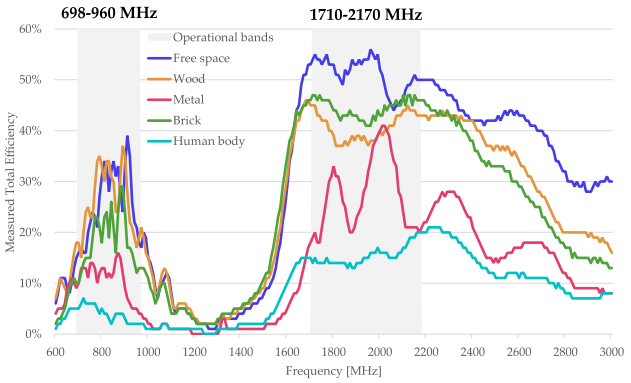

FIGURE 18. Measured total efficiency comparison of optimized switch states. Prototype placed 7 mm on top of all the materials measured in section V.

to the static approach: 1) when the prototype is closer to the material ($h = 7$ mm), and 2) on the materials with a larger relative permittivity (ε_r).

For the first case, when the prototype is 7 mm on top of a phantom body container, at 698-960 MHz, the reconfigurable architecture has an average total efficiency of 4%, which is the worst average total efficiency achieved by the reconfigurable architecture in all measured cases. But in comparison to the 2.7% achieved with the static approach, the reconfigurable architecture has a 1.7 dB better average total efficiency. This difference decreases as the distance to the material h increases by 1 dB for $h = 15$ mm and by 0.5 dB for $h = 20$ mm. This also happens for the rest of the materials. Given that, as the distance h increases, the impact of the material decreases, creating an environment much more similar to the ideal case of free space. That is the reason why the difference between the static approach and the proposed reconfigurable architecture is more equal as the distance h increases.

For the second case, when the prototype is 7 mm on top of a dielectric material, such as wood, brick, or a human body. As the relative permittivity of the given dielectric material increases from the $\varepsilon_r = 1.64$ of wood to the $\varepsilon_r = 3.95$ brick or the $\varepsilon_r = 41.5$ of the human body. The difference between the typical approach and the proposed reconfigurable architecture increases by 0.8 dB for the on-wood case, by 1.7 dB for the on-body case, and by 1.9 dB for the on-brick case. When the prototype is near a high conductivity material, such as aluminum with $\sigma = 3.816 \times 10^7$ S/m, the difference increases to 3 dB. As the impact on the material is more severe, the proposed reconfigurable architecture achieves a better performance.

Despite these differences in cases and for both frequency regions, the proposed reconfigurable architecture has a better average performance than the static approach of using the designed free space architecture for any given environment.

Even though when the prototype is near a conductor, the total efficiency of the proposed reconfigurable architecture

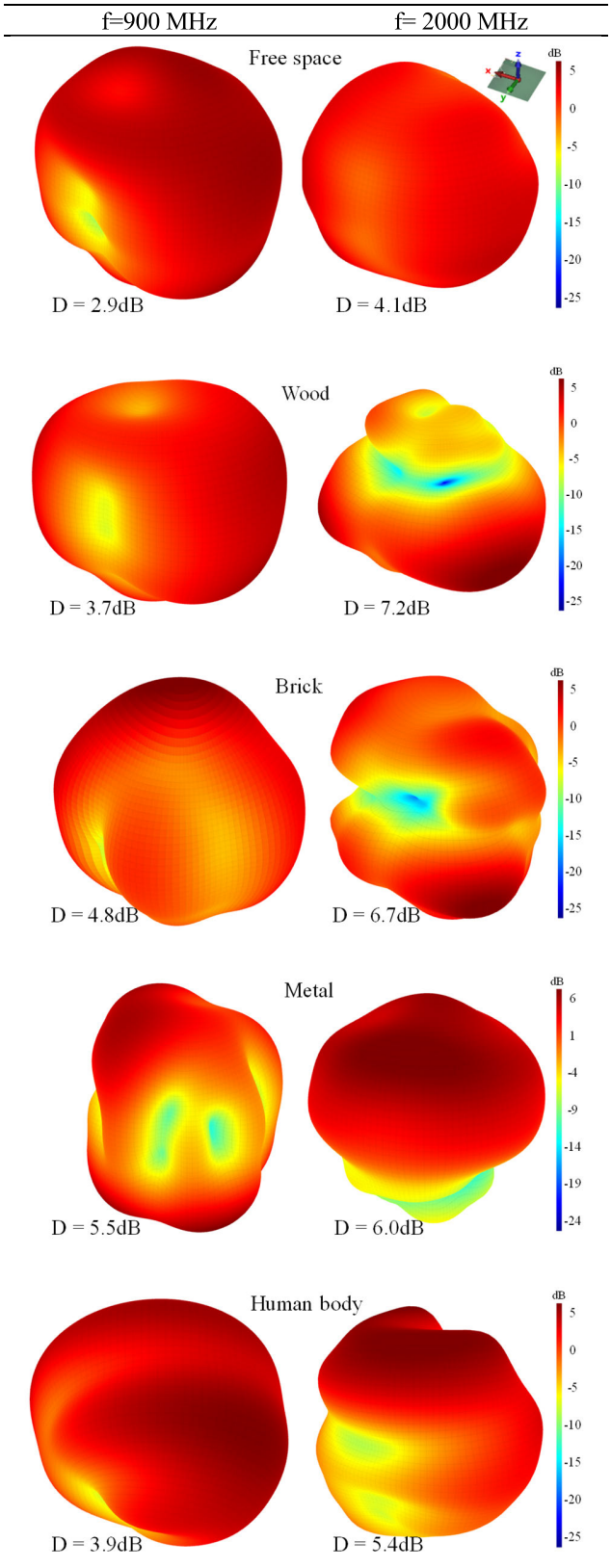

FIGURE 19. Measured radiation patterns.

falls to 10.9% for 698-960 MHz and to 27.7% for 1710-2170 MHz (Fig. 18 – blue), in comparison to free space

TABLE 5. Average measured total efficiency comparison between the typical approach and the proposed reconfigurable architecture.

Average measured total efficiency [%]		698-960 MHz		1710-2170 MHz	
		static approach: Same matching as free space	**Proposed reconfigurable architecture**	**static approach:** same matching as free space	**Proposed reconfigurable architecture**
Free space		26.1	26.1	51.2	51.2
Wood	h = 7 mm	22.2	26.5	39.2	40.5
	h = 15 mm	24.6	25.8	41.0	41.5
	h = 20 mm	24.4	25.3	44.7	45.1
Brick	h = 7 mm	12.3	18.9	42.4	44.4
	h = 15 mm	17.9	20.6	41.9	42.7
	h = 20 mm	21.2	22.6	46.7	47.3
Metal	h = 7 mm	5.1	10.9	18.2	27.7
	h = 15 mm	16.7	19.5	31.2	33.0
	h = 20 mm	24.3	28.1	41.2	45.4
Human body	h = 7 mm	2.7	4.0	15.0	15.4
	h = 15 mm	6.2	7.9	25.7	25.9
	h = 20 mm	8.9	10.0	32.2	32.3

(Fig. 18 – red) for $h = 7$ mm. The material that has a significant impact on the performance of the prototype is a dielectric material, specifically, the human body. With a relative permittivity of $\varepsilon_r = 41.5$, the performance falls to 4.0% and 15.4% (Fig. 18 – light blue), respectively. The same happens with the rest of the h distances (TABLE 5). From those results, when can observe that, even though the frequency shifting produced by a conductor is more severe than the one produced by the dielectric material, as has been discussed. The proposed reconfigurable architecture can mitigate it. What it cannot overcome is the absorption of the dielectric material or the attenuation of the conductor. The obtained results show that the absorption of the human body is larger than the attenuation produced by the presence of a metallic plate.

Finally, radiation patterns are represented for each situation at two representative frequencies of the low and high-frequency bands: 900 MHz and 2000 MHz (FIGURE 19). For the free-space scenario, radiation patterns are quasi-isotropic, featured by low directivity, ensuring reception from any incoming direction of the electromagnetic signals. For other cases (wood, brick, metal, and human body), radiation patterns are slightly modified, in particular for the wood and metal case at 2000 MHz. For this case, the radiation pattern becomes more directive: for the wood case, it increases from 4.1dB of the free-space situation to 7.2dB, pointing to the wood direction. This may be caused by the dielectric loading of the wood acting as a superstrate. This effect is well reported for microstrip patches where a superstrate is used to increase the directivity of the microstrip patch antenna [22].

For the metal case, the impact at 2000 MHz is to increase also directivity. However, the beam is now pointing to the z>0 direction due to the shielding effect of the metallic plane under the wireless device. As a consequence, reception from z<0 is reduced, which depends on the size of the metallic plane.

For the remaining cases, although radiation patterns suffer changes, directivities remain still moderate (<7dB), in particular for the low-frequency bands where the impact in the radiation patterns is less, and thus, reception is quite preserved independently from the angle of arrival of the incoming signal.

VI. CONCLUSION

A reconfigurable multiband architecture with a single SP4T switch and a small multiband antenna booster element able to match in free space and when the prototype is placed on top of four different materials –metallic plate, bricks, wooden plate, and body phantom– using the same topology, has been proposed. The architecture is not only able to properly match independently of the environments ($|S_{11}| < -6$ dB) but also to provide multiband operation at 698-960 MHz and 1710-2170 MHz for a small 50 mm × 50 mm device.

The proposed antenna-booster-based architecture is flexible enough to provide impedance matching across several situations, such as free space, a metallic layer, bricks, wooden plate, and body phantom. As a result, the architecture is robust to the detuning effects due to the environment and, thus, useful to optimize the power consumption of wireless devices.

ACKNOWLEDGMENT

To Qorvo for the samples of the SP4T to build the prototypes.

REFERENCES

[1] L. Mo and H. Zhang, "RFID antenna near the surface of metal," in *Proc. Int. Symp. Microw., Antenna, Propag. EMC Technol. Wireless Commun.*, Hangzhou, China, Aug. 2007, pp. 803–806, doi: 10.1109/MAPE.2007.4393746.

[2] P. Raumonen, L. Sydanheimo, L. Ukkonen, M. Keskilammi, and M. Kivikoski, "Folded dipole antenna near metal plate," in *Proc. IEEE Antennas Propag. Soc. Int. Sym. Digest. Held Conjunct USNC/CNC/URSI North Amer. Radio Sci. Meeting*, Columbus, OH, USA, 2003, pp. 848–851, doi: 10.1109/APS.2003.1217593.

[3] X. Qing and Z. N. Chen, "Proximity effects of metallic environments on high frequency RFID reader antenna: Study and applications," *IEEE Trans. Antennas Propag.*, vol. 55, no. 11, pp. 3105–3111, Nov. 2007, doi: 10.1109/TAP.2007.908575.

[4] L. H. Trinh, F. Ferrero, L. Lizzi, R. Staraj, and J.-M. Ribero, "Reconfigurable antenna for future spectrum reallocations in 5G communications," *IEEE Antennas Wireless Propag. Lett.*, vol. 15, pp. 1297–1300, 2016, doi: 10.1109/LAWP.2015.2505669.

[5] S. Caporal del Barrio, E. Foroozanfard, A. Morris, and G. F. Pedersen, "Tunable handset antenna: Enhancing efficiency on TV white spaces," *IEEE Trans. Antennas Propag.*, vol. 65, no. 4, pp. 2106–2111, Apr. 2017, doi: 10.1109/TAP.2017.2662221.

[6] B. Mun, C. Jung, M.-J. Park, and B. Lee, "A compact frequency-reconfigurable multiband LTE MIMO antenna for laptop applications," *IEEE Antennas Wireless Propag. Lett.*, vol. 13, pp. 1389–1392, 2014, doi: 10.1109/LAWP.2014.2339802.

[7] Y.-L. Ban, S.-C. Sun, P.-P. Li, J. L. Li, and K. Kang, "Compact eight-band frequency reconfigurable antenna for LTE/WWAN tablet computer applications," *IEEE Trans. Antennas Propag.*, vol. 62, no. 1, pp. 471–475, Jan. 2014, doi: 10.1109/TAP.2013.2287522.

[8] J. Ilvonen, R. Valkonen, J. Holopainen, and V. Viikari, "Multi-band frequency reconfigurable 4G handset antenna with MIMO capability," *Prog. Electromagn. Res.*, vol. 148, pp. 233–243, 2014, doi: 10.2528/pier14062703.

[9] C.-M. Peng, I.-F. Chen, and C.-H. Liu, "Multiband printed asymmetric dipole antenna for LTE/WLAN applications," *Int. J. Antennas Propag.*, vol. 2013, pp. 1–6, 2013, doi: 10.1155/2013/704847.

[10] T. Houret, L. Lizzi, F. Ferrero, C. Danchesi, and S. Boudaud, "DTC-enabled frequency-tunable inverted-F antenna for IoT applications," *IEEE Antennas Wireless Propag. Lett.*, vol. 19, no. 2, pp. 307–311, Feb. 2020, doi: 10.1109/lawp.2019.2961114.

[11] C. Zhang, S. Yang, S. El-Ghazaly, A. E. Fathy, and V. K. Nair, "A low-profile branched monopole laptop reconfigurable multiband antenna for wireless applications," *IEEE Antennas Wireless Propag. Lett.*, vol. 8, pp. 216–219, Jun. 2009, doi: 10.1109/LAWP.2008.2007224.

[12] C.-L. Hu, D.-L. Huang, H.-L. Kuo, C.-F. Yang, C.-L. Liao, and S.-T. Lin, "Compact multibranch inverted-F antenna to be embedded in a laptop computer for LTE/WWAN/IMT-E applications," *IEEE Antennas Wireless Propag. Lett.*, vol. 9, pp. 838–841, 2010, doi: 10.1109/LAWP.2010.2069079.

[13] H. Li, J. Xiong, Y. Yu, and S. He, "A simple compact reconfigurable slot antenna with a very wide tuning range," *IEEE Trans. Antennas Propag.*, vol. 58, no. 11, pp. 3725–3728, Nov. 2010, doi: 10.1109/TAP.2010.2071347.

[14] Y. Li, Z. Zhang, J. Zheng, and Z. Feng, "Compact heptaband reconfigurable loop antenna for mobile handset," *IEEE Antennas Wireless Propag. Lett.*, vol. 10, pp. 1162–1165, 2011, doi: 10.1109/LAWP.2011.2171311.

[15] J. Anguera, A. Andújar, C. Puente, and R. Mateos, "Modular multi-stage antenna system for wireless communications," U.S. Patent 11 482 772 B2, Oct. 25, 2022.

[16] J. Anguera, A. Andujar, G. Mestre, J. Rahola, and J. Juntunen, "Design of multiband antenna systems for wireless devices using antenna boosters [application notes]," *IEEE Microw. Mag.*, vol. 20, no. 12, pp. 102–114, Dec. 2019, doi: 10.1109/MMM.2019.2941662.

[17] A. Fernández, J. Rahola, J. Juntunen, A. Andújar, J. L. Pijoan, and J. Anguera, "Embedding antenna booster in smart-metering platforms," in *Proc. 16th Eur. Conf. Antennas Propag. (EuCAP)*, Madrid, Spain, Mar. 2022, pp. 1–4, doi: 10.23919/EuCAP53622.2022.9769182.

[18] J. Anguera, C. Picher, A. Bujalance, and A. Andújar, "Ground plane booster antenna technology for smartphones and tablets," *Microw. Opt. Technol. Lett.*, vol. 58, no. 6, pp. 1289–1294, Mar. 2016, doi: 10.1002/mop.29788.

[19] Ignion. (Apr. 12, 2022). *Trio mXTEND^{TM} Multiband Antenna*. Accessed: Mar. 8, 2023. [Online]. Available: https://ignion.io/product/trio-mxtend/

[20] C. A. Balanis, *Antenna Theory: Analysis and Design*. Chichester, U.K.: Wiley Blackwell, 2016.

[21] J. Anguera, A. Andújar, and C. Puente, "Multiband antenna booster architecture with a single switch," U.S. Patent Appl. 2022/0 376 722 A1, Nov. 24, 2022.

[22] D. Jackson and N. Alexopoulos, "Gain enhancement methods for printed circuit antennas," *IEEE Trans. Antennas Propag.*, vol. AP-33, no. 9, pp. 976–987, Sep. 1985, doi: 10.1109/TAP.1985.1143709.

ALEJANDRO FERNÁNDEZ received the B.Sc. degree in telecommunication systems engineering and the M.Sc. degree in telecommunication engineering from La Salle, Ramon Llull University, in 2020 and 2021, respectively. He is currently pursuing the Industrial Ph.D. degree with La Salle, Ramon Llull University, and Ignion. He was supported in part by the Industrial Doctorate Plan of the Secretariat of Universities and Research of the Department of Business and Knowledge of the Generalitat of Catalonia under reference 2021 DI 115. He is currently a Research and Development Engineer with Ignion. He has published related to his doctoral thesis in various journals and international conferences. His current research interests include antenna boosters and reconfigurable antenna solutions.

AURORA ANDÚJAR was born in Barcelona, Spain. She received the bachelor's, master's, and Ph.D. degrees in telecommunication engineering from Universitat Politècnica de Catalunya (UPC), in 2005, 2007, and 2013, respectively.

From 2004 to 2005, she was a Research Fellow of electromagnetic compatibility from the Signal Theory and Communications Department, UPC. In 2005, she was a software test engineer for applications intended for handset wireless devices. In 2006, she was a Software Engineer designing a load simulation tool for testing Digital Campus in academic environments and developing improvements in the performance of web servers referred to the management of static and dynamic contents. From 2007 to 2017, she was a Research and Development Engineer with Fractus, where she was in charge of the development of technological projects focused on the design of miniature and multiband antennas for wireless devices. She was also involved in the maintenance and growth of the patent portfolio of the company, including the development, writing, and prosecution of new inventions and patents, from 2007 to 2013. Since 2009, she has been leading research projects in the antenna field for wireless devices in the collaborative university-industry framework. In 2013, she moved to the Products and Service Department, where she was in charge of the development and release of new antenna products for wireless devices. Since 2015, she has been the Director of engineering with Ignion, where she is leading the development and management of the company's products and services. She is Co-Founder of Ignion. She has more than 16 years of experience in the antenna industry. She is an inventor of more than 55 patents in the antenna field. She has published more than 100 papers in scientific journals, international, and national conferences. She has directed more than 60 bachelor's and master's thesis.

Dr. Andújar received two awards for the Best Ph.D. Thesis given by Colegio Oficial Ingenieros de Telecomunicación (COIT) and the Special Award given by UPC.

JOAN LLUÍS PIJOAN received the bachelor's degree in telecommunications technical engineering from La Salle, Ramon Llull University, in 1991, the master's degree in telecommunications engineering from the Polytechnic University of Catalonia, in 1994, and the Ph.D. degree in electronics from Ramon Llull University (URL), in 2000.

Since 1998, he has been a Professor with the La Salle School of Electronic and Computer Engineering (Ramon Llull University), Department of Communications and Signal Theory. Since 2003, he has been investigating the use of broadband modulations in long-distance HF links between Antarctica and Spain; and the daily, seasonal, and annual variation of the parameters that characterize the ionosphere as a communication channel. Since 2013, he has experimented with using the near vertical incidence skywave (NVIS) technique for remote sensing and designing compact HF antennas. He was the Head of the Department of Communications and Signal Theory, Ramon Llull University, from 2001 to 2011; and the Head of the Research Group on Electromagnetism and Communications (GRECO), Ramon Llull University, from 2000 to 2013, a consolidated group recognized by the Generalitat de Catalunya, in 2009. Due to a reorganization of the research groups, he belonged to the Research Group on Internet and Storage Technologies (GRITS), URL, from 2016 to 2022. In 2004, he received the Accreditation of a Lecturer by the Quality Agency of the Catalan University System (AQU), where he also received the Accreditation of Research, in 2011. He has also been granted the six years research periods, from 2004 to 2009, from 2010 to 2015, and from 2016 to 2021. In 2017, he was a Full Professor with Ramon Llull University. He is currently the Coordinator of the degree in telecommunications systems engineering with URL. He also belongs to the recently recognized Research Group on Smart Society. He is the author of more than 30 articles in magazines and more than 70 contributions at conferences. He has directed eight doctoral thesis and more than 190 final degree projects. He has participated in 26 public and private research projects, being the principal investigator in 19 of them. He has also actively participated in the European stocks COST 262 Spread Spectrum Systems and Techniques in Wireless and Wired Communications and COST 289 Spectrum and Power Efficient Broadband Communications. He has participated as a reviewer for national and international scientific and technical publications and projects. His current research interests include channel sounding and modeling, the design of spread spectrum and multi-carrier modulations applied to broadband HF communications and power line communications, and the design of multi-user detectors in CDMA systems.

JAUME ANGUERA (Fellow, IEEE) was born in Vinaròs, Spain, in 1972. He received the Technical Engineering in Electronic Systems and Engineering degrees in electronic engineering from Ramon Llull University (URL), Barcelona, Spain, in 1994 and 1998, respectively, and the Telecommunication Engineering (5 years degree) and Ph.D. degrees in telecommunications from the Polytechnic University of Catalonia (UPC), Barcelona, in 1998 and 2003, respectively.

From 1997 to 1999, he was a Researcher of microstrip fractal-shaped antennas with the Electromagnetic and Photonic Engineering Group, Signal Theory and Communications Department, UPC. In 1999, he was a Researcher with Sistemas Radiantes, Madrid, Spain, where he was involved in designing dual-band dual-polarized fractal-inspired microstrip patch arrays for mobile communications. In 1999, he was an Assistant Professor with the Department of Electronics and Telecommunications, Universitat Ramon Llull, and an Associate Professor, in 2016, where he is currently teaching antenna theory related courses and belong to the recognized Research Group on Smart Sociey. Since 2001, he has led research projects in the antenna field for wireless applications in a frame of industry-university collaboration: Ignion and the Department of Electronics and Telecommunications, Universitat Ramon Llull. Several of his supervised students have been awarded Best Bachelor's and Master's Thesis by the Spanish Ministry and other Spanish institutions. From 1999 to 2017, he was with Fractus (founder partner), Barcelona, where he was the Research and Development Manager and developed various cutting-edge antenna technologies. At Fractus, he led projects on antennas for base station systems antennas for automotive. From 2003 to 2006, he was also assigned to Fractus, South Korea, to head up the research team. One of his main tasks was to provide training, education, and development of the team's core competency and provide a research and development vision to address the rapidly growing mobile device market. Under his leadership, the company had secured major contracts with companies, such as Samsung, LG, and Bellwave, to name a few. Since 2017, he has been the CTO with Ignion, where he is Co-Founder. He is also an Associate Professor with Universitat Ramon Llull. He leads the company's research and development activity to create new products, envisages new technologies, and provides technology strategy and direction to scale the company's business. He published a book about *Korean Experiences* in 2015. He holds more than 170 granted invention patents (the USA, Asia, and Europe) in the antenna field, many of which have been licensed to the wireless industry. Among his most outstanding contributions is that of the inventor of antenna booster technology, a technology that fostered the creation of Ignion. The wireless industry has adopted many of these products worldwide to allow wireless connectivity to the IoT devices through a miniature component called an antenna booster that is ten times smaller than conventional antennas. He is the author of more than 280 journals and international and national conference papers (h-index of 55 and with more than 9000 citations based on Google Scholar). He has given more than 50 antenna lectures worldwide (the USA, China, Korea, India, the U.K., France, Poland, Czech Republic, Tunisia, Perú, Brazil, Canada, and Spain). He has directed more than 160 bachelor's, master's, and Ph.D. thesis. He has authored seven books. He has participated in more than 20 national/international projects and research grants valued at more than $13 million, of which he was the principal researcher in many of them. His current research interests include antenna boosters, multiband and small antennas, diversity antenna systems/MIMO, electromagnetic dosimetry, microstrip antennas, and genetically optimized antennas.

Dr. Anguera was a member of the Fractal Team that, in 1998, received the European Information Technology Grand Prize for Applied Science and Engineering for the fractal-shaped antenna application to cellular telephony. The 2003 Finalist for the Best Doctoral Thesis on UMTS (Fractal and Broadband Techniques on Miniature, Multifrequency, and High-Directivity Microstrip Patch Antennas; prize promoted by ''Technology plan of UMTS promotion'' given by Telefónica Móviles España). The 2004 New Faces of Engineering (promoted by IEEE and IEEE foundation). In 2004, he won the Best Doctoral Thesis (Ph.D.) in ''Network and Broadband Services'' (XXIV Prize Edition ''Ingenieros de Telecomunicación'') organized by Colegio Oficial de Ingenieros de Telecomunicación (COIT) and the Company ONO (National Price). In 2011, he received Alè Vinarossenc Recognition from Fundació Caixa Vinaròs. In 2014, he received the 2014 Finalist for European Patent Award, along with four other Fractus inventors. He is a reviewer for several IEEE journals and others. He is an Associate Editor of IEEE Open Journal on Antennas and Propagation and *Electronics Letters*. His biography is listed in Who's Who in the World, Who's Who in Science and Engineering, Who's Who in Emerging Leaders, and International Biographical Center (IBC), Cambridge, England. He is an IEEE Antennas and Propagation Distinguished Lecturer. He is the Working Group ''Software and Modeling'' Vice-Chair at EurAAP. His detailed information can be found at: http://users.salleurl.edu/~jaume.anguera/